Catalytic Activity of Carbon-Supported Pt Nanoelectrocatalysts. Why Reducing the Size of Pt Nanoparticles is Not Always Beneficial

ARTICLE *in* THE JOURNAL OF PHYSICAL CHEMISTRY C · APRIL 2011

Impact Factor: 4.77 · DOI: 10.1021/jp1109477

6 AUTHORS, INCLUDING:

I. N. Leontyev
Southern Federal University
29 PUBLICATIONS **136** CITATIONS
SEE PROFILE

Sergey V. Belenov
Southern Federal University
8 PUBLICATIONS **62** CITATIONS
SEE PROFILE

V.E. Guterman
Southern Federal University
34 PUBLICATIONS **195** CITATIONS
SEE PROFILE

Brahim Dkhil
Ecole Centrale Paris
205 PUBLICATIONS **4,485** CITATIONS
SEE PROFILE

THE JOURNAL OF PHYSICAL CHEMISTRY C

ARTICLE

pubs.acs.org/JPCC

Catalytic Activity of Carbon-Supported Pt Nanoelectrocatalysts. Why Reducing the Size of Pt Nanoparticles is Not Always Beneficial

I. N. Leontyev,*[,†,‡] S. V. Belenov,[§] V. E. Guterman,[§] P. Haghi-Ashtiani,[⊥] A. P. Shaganov,[¶] and B. Dkhil[†]

[†]Laboratoire Structures, Propriétés et Modélisation des Solides, CNRS UMR 8580 École Centrale Paris, 92295 Châtenay-Malabry Cedex, France

[‡]Faculty of Physics, Southern Federal University, 5 Zorge Street, Rostov-on-Don 344090, Russia

[§]Faculty of Chemistry, Southern Federal University, 7 Zorge st, Rostov-on-Don 344090, Russia

[⊥]Laboratoire de Mécanique des Sols, Structures et Matériaux École Centrale Paris, 92295 Châtenay-Malabry Cedex, France

[¶]Polytechnical University, Radiophysical Science and Engineering Faculty, 29 Polytechnicheskaya st, St.Petersburg, 195251, Russia

ABSTRACT: Carbon-supported Pt catalysts prepared by the impregnation method in water−dimethyl sulfoxide (DMSO) solutions were investigated. Using X-ray diffraction (XRD) technique for estimation of the particle size and shapes, we show that morphology of the Pt/C catalysts depends strongly on the DMSO content in the solutions. The average particles size reduces and a shape of the Pt nanocrystals changes from a truncated octahedron to a cuboctahedron and eventually to a truncated cube with increasing DMSO concentration in the reaction mixture. Antibate effects of the size and shape cause nonmonotonic dependence of the catalytic activity for the oxygen reduction reaction (ORR) with electric current maximum at an average particle size of 2.7 nm.

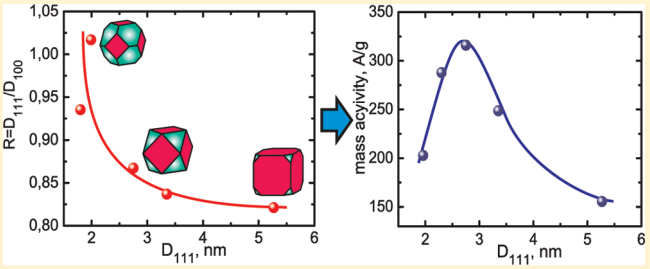

Properties of the nanoparticles have been studied extensively both in catalysis and electrocatalysis.[1] In the latter case, these studies have been carried out with two main objectives: (i) understanding of fundamental aspects of the surface electrochemical activity and (ii) the development of new materials for practical applications, for example, in fuel cells. Despite the high cost, Pt and its alloys are among the most promising candidates both for cathode and anode catalysts in the fuel cell applications.

The average Pt particle size in a catalyst falls typically in the range of 2−10 nm, and it is well-known that the activity of a Pt/C catalyst for the oxygen reduction reaction (ORR) depends greatly on the particle size (so-called size effect). The particle size effect of Pt/C in the ORR has been well documented.[2−6] However, contradictory results have been obtained. More frequently, the catalytic activity enhances with reduction in the average particle size (direct, or positive size effect).[2] Meanwhile, manifestations of the inverse (negative) size effect are also observed where the activity reduces as the particles become smaller.[3] Moreover, there has been an example where the activity was found to be independent of the particle size.[4] There have been many attempts to elucidate the factors affecting the ORR catalytic activity of the Pt-based catalysts (such as the Pt−Pt distance, the coordination number of Pt, and electron density of states in the Pt 5d band), but some debate has still remained on the detailed mechanisms involved. In this work, the electrocatalytic activity of the carbon-supported Pt catalysts was investigated as a function of both the particle size and shape. We demonstrate that the observed discrepancies could be due to changes in the particle shape accompanying changes in the particle size.

The catalysts were prepared by a classic chemical reduction method, in which a water−organic solvent was employed instead of water.[7] By varying the solvent composition, we obtained catalysts with different structural and microstructural characteristics. In particular, both the nature of the components and their concentration affect (i) the surface wettability of the carbon support, (ii) adsorption of the precursors, and (iii) the structure of solvate complexes of metals and their redox potentials. These factors also determine the solution viscosity and mass transfer of the reagents to the carbon support particles.[6] All these effects, in turn, influence on nucleation and growth of the nanoparticles and hence on the characteristics of the finished samples. Therefore, we examaine the influence of the water−DMSO solvent composition on the micro structural parameters of the Pt/C materials.

EXPERIMENTAL SECTION

Sample Preparation. Pt/C catalysts were prepared by the impregnation method using $H_2PtCl_6 \cdot 6H_2O$ (Aurat, Russia) as a precursor, 0.5 M $NaBH_4$ as a reducing agent, and H_2O−DMSO as a solvent (a more detailed description of the preparation procedure can be found in ref 8). Five Pt/C samples synthesized using DMSO concentrations of 0%, 17%, 50%, 65%, 83% by volume in the solvent were denoted as PT00, PT17, PT50, PT65, PT83,

Received: November 16, 2010
Revised: January 16, 2011
Published: March 04, 2011

respectively. A carbon black powder (VULCAN XC72, Cabot Corp. 240 m^2/g) was used as a support. pH of the H_2O−DMSO solution was raised to 10 by adding ammonium saturated water solution. During the synthesis, the suspension was mixed by ultrasonic blending. Finally, the suspension was filtered, washed, and dried in air (100−120 °C, 2−3 h.). At the end of the treatment, each catalyst had a metal loading of approximately 20 wt %.

X-ray Diffraction (XRD). Powder diffraction patterns were recorded at the Swiss-Norwegian Beamlines (SNBL) at the European Synchrotron Radiation Facilities (ESRF) at λ = 0.77 Å using a MAR345 image-plate detector. The wavelength, sample-to-detector distance (95 mm), and resolution of the setup were calibrated with LaB_6 (NIST) powder.[9] Samples were placed into glass capillaries (Hilgenberg GmbH) having a diameter of 0.3 mm and a wall thickness of 0.01 mm. The data were processed with the *Fit2D* software.[10] The peak shapes were described using the pseudo-Voigt function.[11] The X-ray reflections were fitted using the Winplotr from the *FullProf* software.[12] Fittings of the reflections from the synthesized samples were made with allowance for the reflections from the carbon support.[13] Corrections for the instrumental line broadening were made according to a conventional procedure described in ref 14.

The average particle size was determined as usually by the well-known Scherrer equation:[15] $\overline{D} = K\lambda/(\text{fwhm} \cos\theta)$, where λ is the wavelength, $\overline{D}$ is the volume averaged particle size, $K = 0.89$ is the Scherrer constant, fwhm is the full width at half-maximum of the peak, and θ, the Bragg angle of the $[hkl]$ reflection. However, this equation neglects the strain, which can contribute to the broadening of the Bragg peak. Therefore, a second method, developed by Williamson and Hall,[16] now known as the Williamson−Hall plot (WH), was also used. In this more complete approach, fwhm is plotted as a function of $(2 \sin\theta/\lambda)$ for all the Bragg reflections for each sample, expressed in terms of reciprocal units, $(\text{fwhm} \cos\theta/\lambda)$. Using a linear extrapolation of the measured points, the intersection with the vertical axis gives the particle size $(K/\overline{D})$, whereas the slope gives the strain. One may remark that, for strain-free grains, the WH method becomes equivalent to the Scherrer approach.

In addition, the so-called $FW^1/_5/^4/_5M$ method was also used to determine parameters of the grain size distribution (GSD), that is the grain size dispersion around its average value. A detailed description and justification of this method can be found in ref 17. The second method is based on the assumption that the grain size distribution GSD obeys a Gamma function

$$\mathrm{GSD}(D: D_0, m) = \frac{D_0^{-m-1}}{\Gamma(m+1)} D^m \exp(D/D_0)$$

where $D_0 = \sigma^2/\overline{D}$, $m = (\overline{D}/\sigma)^2 - 1$, which is very close to the conventional log-normal distribution. The average particle size $\overline{D}$ and its dispersion σ were derived from the expressions

$$\overline{D} = 2\mathrm{BC}/\mathrm{FW}\frac{4}{5}\mathrm{M}, \sigma = 2\mathrm{B}\sqrt{C}/\mathrm{FW}\frac{4}{5}\mathrm{M}$$

The coefficients B and C were found from the expressions

$$\mathrm{A} = \mathrm{arcctg}\left(277\,069 - 105\,723\mathrm{FW}\frac{1}{5}\mathrm{M}/\mathrm{FW}\frac{4}{5}\mathrm{M}\right)$$

$$\mathrm{B} = 0.001555 + 0.00884 \times \mathrm{ctg}(0.002237 - 2101 \times \mathrm{A})$$

$$\mathrm{C} = -0.6515 - 463\,695 \times \mathrm{A}$$

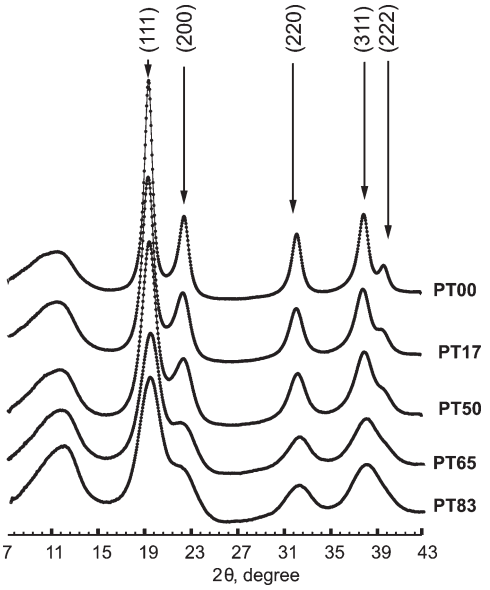

Figure 1. XRD patterns of the Pt/C catalysts.

where $FW^1/_5M$ and $FW^4/_5M$ are the full widths at 1/5 and 4/5 of the peak maximum, respectively. For determination of the GSD parameters by this method, we used the available *LTGSD* program.[18]

Finally, the fitting results for the ⟨111⟩ and ⟨200⟩ peaks were used for determination of the average particle size and the GSD parameters using the Scherrer equation and the method. The results for the ⟨111⟩ and ⟨222⟩ peaks were used in the Williamson−Hall method. Finally, all reflections of the powder diffraction pattern were used for calculation of the unit cell parameter by means of the *UNITCELL* software.[19]

Electrochemical Characterization. All electrochemical measurements were performed using a standard three-electrode electrochemical cell with a IPC-Pro potentiostat (Volta Ltd.). Electrochemical properties of the Pt/C catalysts were determined using a rotating disk electrode (RDE) that consisted of a glassy carbon (GC) disk sealed in a polytetrafluoroethylene holder. The geometric surface area of the disk electrode was 0.28 cm^2 (diameter:, 6 mm). The RDE was polished to a mirror finish with a 0.05 mm alumina suspension and then cleaned ultrasonically in highly pure water. On top of this layer, the electrocatalyst was applied in form of a homogeneous dispersion (catalyst ink). Catalyst inks were prepared with 7 mg of a catalyst, 80 μL of water, 140 μL of 10% polyvinilidenfluoride emulsion in *N*-methyl-2-pyrrolidone and 800 μL of isopropanol. After ultrasonic dispergation, an ink volume of 3.5 μL was dropped onto a GC electrode and dried initially at room temperature and subsequently at 100 °C.[20] The potentials cited in this work are referred to that of the RHE. To identify the ORR activities of the carbon-supported electrocatalysts, cyclic voltammetry (CV) was conducted in the potential range 0.05−1.2 V at a scan rate of 20 mV^*s^{-1} with a rotation speed of 1000 rpm. The electrolyte was a 1 M H_2SO_4 (Merck) solution saturated with oxygen (p = 1 atm). Sulfuric acid was chosen because, even after taking into account complications caused by the specific adsorption of SO_4^{2-} anions in this electrolyte, it was easier to compare the results with the literature data. All measurements were carried out at room temperature. A commercial Pt/C catalyst from E-TEK (20% metal loading on Vulcan XC72, D_{111} = 2.3 nm) was measured for comparison.

dx.doi.org/10.1021/jp1109477 |J. Phys. Chem. C 2011, 115, 5429–5434

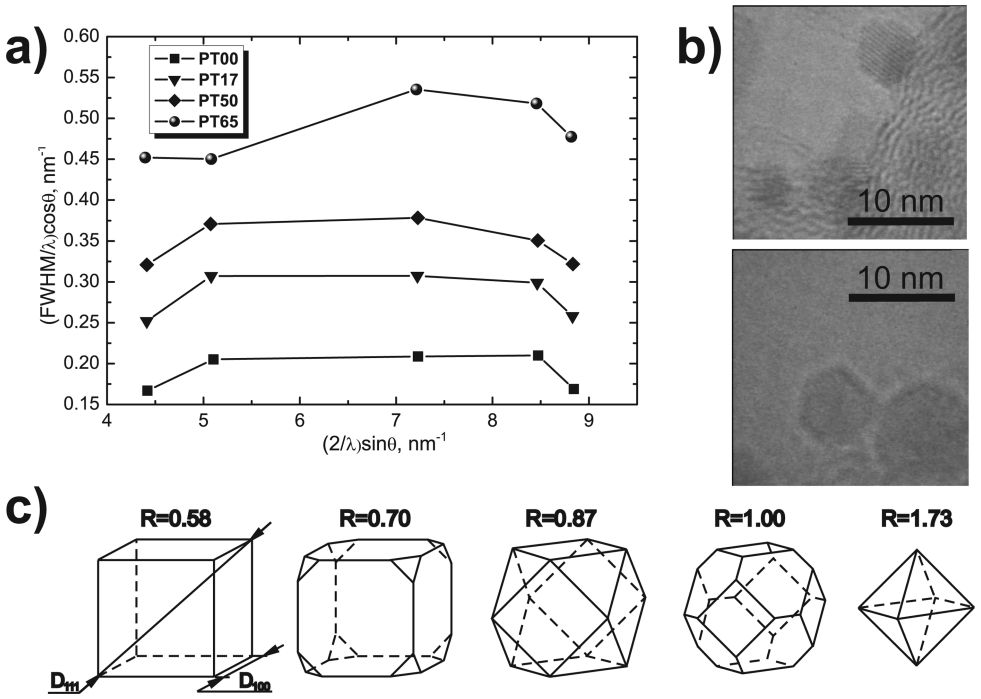

Figure 2. (a) Williamson−Hall plot, (b) high-resolution TEM micrographs for the prepared Pt/C electrocatalysts (PT50), and (c) schematic illustration of different polyhedrons for nanoparticle shapes of the fcc metals; from left to right: cube, truncated cube, cuboctahedron, truncated octahedron, octahedron, respectively, and their anisotropic factor.

RESULTS AND DISCUSSION

XRD powder patterns of the synthesized Pt/C catalyst are shown in Figure 1. For all of the samples, only the reflections corresponding to the face centered cubic (fcc) structure are observed. Part a of Figure 2 displays the Williamson−Hall (WH) plot for the synthesized materials. It is obvious that no straight line could provide an acceptable extrapolation of the experimental data. Furthermore, the {*hhh*} reflections have consistently lower fwhm's compared to the other ones. Part a of Figure 2 rather reflects the existence of anisotropy on the lines broadening meaning that along the different crystallographic directions the size/strain is different. As a consequence, the WH plot should be considered for each crystallographic family. Unfortunately, because of the few number of Bragg peaks, this treatment can be only done for the (hhh) family using both (111) and (222) reflections. Interestingly, the straight line obtained using these two latter reflections is roughly horizontal meaning that the slope, or, in other words, the strain is close to zero. Therefore, the strain contribution to the line broadening could be considered as negligible and the Scherrer equation[15] and the $FW^1/_5/^4/_5M$ method[17] are then, here, applicable for the determination of the particles size and the GSD parameters. Moreover, usually in metals, this anisotropy of line broadening may be attributed to specific crystallite shape (anisotropy), presence of dislocations or stalking faults. The high-resolution TEM images, depicted in part b of Figure 2, clearly evidence a strong anisotropy of the particles. Absence of dislocations in such prepared catalysts is also confirmed by previous results[21] in which it has been shown that the particles became dislocation-free below a certain critical size. For instance, dislocation-free particles of copper and nickel have diameters of 38 and 16 nm, respectively.[21] It is worth mentioning that, as illustrated in numerous review articles,[22] for an fcc metal, the nanoparticles shape commonly observed in the fcc metals can be divided into two categories: single and twinned nanocrystals. Single crystalline structures or Wullf's polyhedra represent perfect polyhedra (cubes, octahedra) and their truncated modifications (a truncated cube (TC), a cuboctahedron (CO) or a truncated octahedron (TO)). The twinned nanocrystals rather assume the forms of decahedra or icosahedra. Pt nanoparticles synthesized by many authors have typically a single crystalline structure also observed for our catalysts (part b of Figure 2). The shape of Wullf's polyhedra (part c of Figure 2) can be determined by the ratio $R = D_{100}/D_{111}$ (the anisotropy factor) that is the ratio of the growth rates along the ⟨100⟩ and ⟨111⟩ directions. An octahedron bounded by the lowest-energy closepacked {111} facets has $R = 1.73$. A cube has $R = 0.58$ and is enclosed by only {100} faces (part c of Figure 2); the latter have a higher surface energy in most materials.[23] Various truncated versions of octahedra and cubes have intermediate R values and are bounded by both the {111} and {100} facets (part c of Figure 2). Summarizing the aforesaid, it is possible to characterize a change in the shape of Pt nanoparticles in the synthesized catalysts using the fwhm ratio for the (111) and (200) reflections (it should be noted that it is valid in cases where the line broadening is due to the particle size alone). The resulting anisotropy factor $R_v = D_{100}/D_{111} = \mathrm{fwhm}_{111} \cos(\theta_{200})/\mathrm{fwhm}_{200} \cos(\theta_{111})$ will characterize the volume-averaged particles shape of a sample. Such an unconventional approach to the shape characterization has advantages over the usually employed TEM methods.[16] Indeed, the X-ray equipment can generally be found in many laboratories and this technique allows analyzing a large volume with many nanoparticles while, in contrast, TEM provides only data from a very small area of a Metal/C catalyst. A wide X-ray beam can cover up to 10^{11} times more nanoparticles than an electron beam.

Characteristics of the prepared catalysts, derived from the XRD data, are summarized in Table 1. The average particle sizes along the ⟨111⟩ direction, D_{111}, calculated using the Scherrer

dx.doi.org/10.1021/jp1109477 |J. Phys. Chem. C 2011, 115, 5429–5434

Table 1. Characteristics of Carbon-Supported Pt Catalysts[a]

			Scherrer			WH	$FW^1/_5/^4/_5M$		
sample	DMSO concentration	metal loading	D_{111}	D_{200}	D_{200}/D_{111}	D_{111}	D_{111}	σ	a
PT00	**0**	21	5.27	4.35	0.821	5.40	5.21	3.10	3.911
PT17	**0.17**	21	3.35	2.82	0.837	3.54	3.46	2.00	3.910
PT50	**0.50**	19	2.75	2.40	0.867	2.78	2.84	1.53	3.903
PT65	**0.65**	20	1.96	1.92	1.008	2.08	2.10	1.05	3.896
PT83	**0.83**	21	1.76	1.81	0.968		2.02	0.8	3.874

[a] DMSO concentration in the solvent (%), metal loading (wt%), average particle sizes D_{111}, D_{200} along the ⟨111⟩ and ⟨200⟩ directions and GSD dispersion σ (nm), unit cell parameter a (Å).

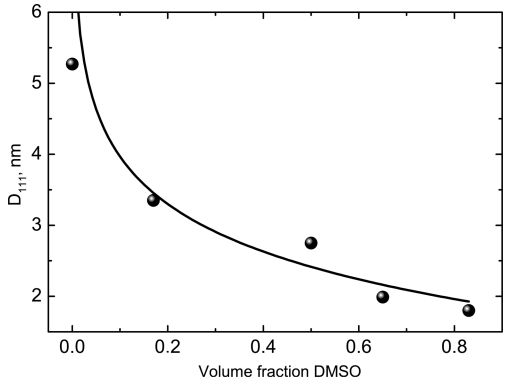

Figure 3. Average particle size along ⟨111⟩ direction D_{111} as function of the DMSO volume fraction. The solid line is a guide for the eyes.

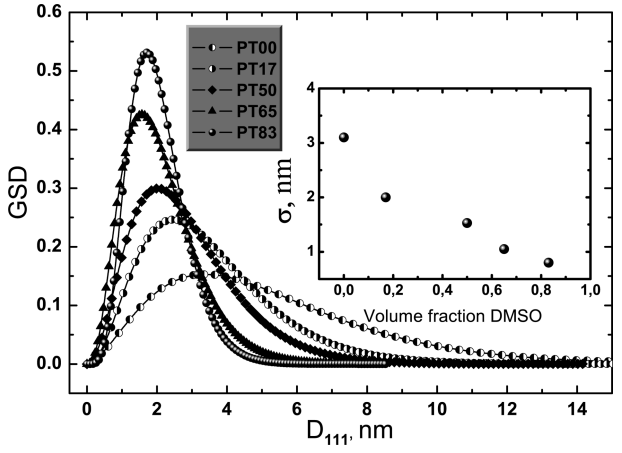

Figure 4. Grain size distribution (GSD) in the prepared Pt/C electrocatalysts determined by XRD using the FW $^1/_5/^4/_5$ M method. Insert: Dispersion σ as a function of DMSO volume fraction.

equation[15] and the WH plot[16] were found, as expected, to be very similar and close to that determined by the $FW^1/_5/^4/_5M$ method. As the DSMO concentration was lowered, D_{111} increased from 1.8 to 5.4 nm (Table 1). The same trend was observed for D_{200}, which was found to vary between 1.8 and 4.3 nm, being always smaller than quasi-equal to D_{111}.

The DMSO concentration dependence of D_{111} is presented in Figure 3. As already mentioned, D_{111} increases with lower concentrations of the organic component in the solvent. The strongest effect of the solvent composition is found in the 0−20% DMSO concentration range. A similar effect is observed for

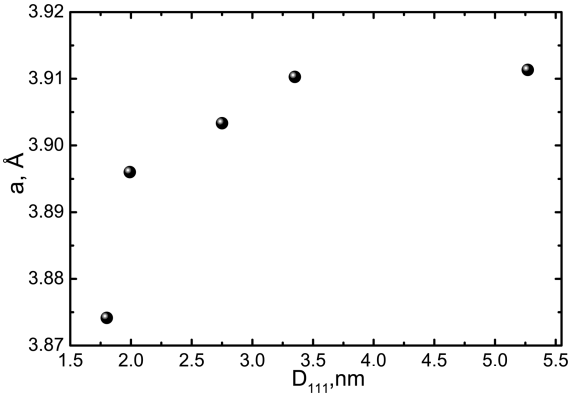

Figure 5. Lattice parameter a as function of average particle size along the ⟨111⟩ direction, D_{111}, for Pt/C electrocatalysts.

Pt_3Co/C electrocatalysts prepared using a water−ethylene glycol solvent.[13] The narrowest GSD is found for the smallest particles synthesized at a DMSO concentration of 83% (Figure 4). This means that, in the specified conditions, the nucleation prevails over the particle growth, which corresponds to the instantaneous nucleation model. Increasing the H_2O content in the solvent favors the growth process, which in turn leads to a larger particle size and wider GSD (Figures 3 and 4). We already noted there are many variable factors that affect the nucleation/growth processes when the solvent composition changes. Unfortunately, we are lacking our experimental and the literature data that could determine a character of the dependence of these important factors (e.g., the precursor adsorption, the surface wettability, the solvation sphere composition, etc.) on the water−DMSO solvent composition. The unit cell parameter a of the prepared catalysts decreases with reduction in the average particle size (Figure 5). The lattice contraction can be explained in terms of a surface stress,[25] which makes the unit cell more compact as it has been observed for nanoparticles of the fcc metals other than Pt.[26] More interestingly, we also found that the DMSO concentration affects morphology of the nanoparticles. The R-factor for the sample PT83 (Table 1) corresponds to that for TO shape. This fact and the narrowest GSD for that sample indicate that a shape of the nanocrystallite seeds may be assumed to be TO. It is noteworthy that this $R = 1$ corresponds to a sphere. The formation of such particles may be explained by the fact that the shape of a nucleus is primarily determined by minimization of the surface energy. As dictated by thermodynamics, TO is the most favorable shape because of its small surface area and low surface energy.[27]

As the DMSO concentration is lowered and the particles become larger, the R_v-factor increases and the shape of the Pt

dx.doi.org/10.1021/jp1109477 |J. Phys. Chem. C 2011, 115, 5429–5434

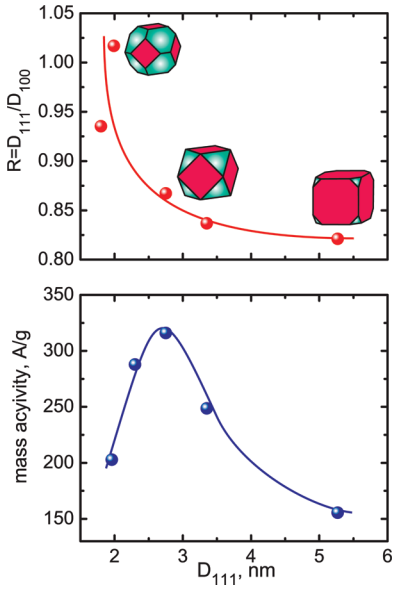

Figure 6. Anisotropy factor R (upper panel) and mass activity of Pt/C catalysts at E = 0.7 V for ORR (lower panel) as functions of average particle size along the ⟨111⟩, D_{111}. Solid lines are the guides for eyes.

nanoparticles changes from TO to CO, and eventually to TC (Figure 6). Therefore after the nucleation stage, Pt atoms are continuously deposited onto the {111} facets, which results in selective growth along the ⟨111⟩ direction. It is well-known that impurities or capping agents presented in a solution can play a key role in nucleation and growth of the particles. We suppose that adsorption of the DMSO molecules at the nanoparticles facets inhibits the attachment of Pt atoms evolved during the reaction and thereby increases the crystal growth activation energy. In the solutions with low organic component concentrations, the DMSO molecules are adsorbed preferably at the more sensitive {100} facets. As a result, the {100} facets became more accessible to the new Pt atoms, leading to a preferred nanoparticle growth along the ⟨111⟩ direction and an increasing fraction of the surface corresponding to the (100) planes. The shape of such nanoparticles approaches TC. At higher organic component concentrations, the DMSO adsorption enhances and becomes more uniform at the same time. The ⟨111⟩ to ⟨100⟩ growth rate ratio then becomes closer to unity and the growth itself is inhibited further. The nanoparticle being formed in such solutions grow homotetically retaining both the {111} and {100} facets. They are smaller and their shape is closer to CO or TO.

Cyclic voltamperograms recorded with the RDE for the prepared Pt/C and commercial E-TEC20 catalysts in the potential range of 0.6−0.8 V indicate that the catalyst with D_{111} = 2.75 nm prepared in an H_2O−DMSO solvent with the 1:1 component ratio shows the best mass activity (Figures 7 and 8). At E = 0.7 V, its specific current was 1.15 times that of the E-TEC20 counterpart, whereas the ORR activity of the remaining samples was lower by factors of 1.5−2.0. Note that, at E = 0.7 V, current values for all of the studied catalysts became constant already after the second cycle, some of them demonstrating even a slight gain in the ORR activity.

As already mentioned, higher DMSO concentrations provoke a reduction in the average particle size D_{111}, a decrease in the GSD dispersion and in the unit cell parameter. This combined effect would result in a monotonic increase in the catalytic

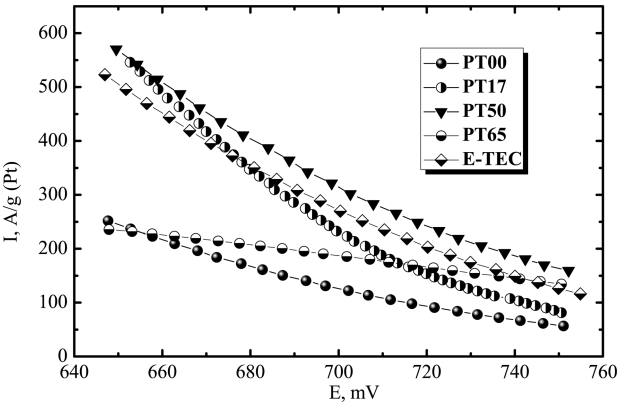

Figure 7. Sections of polarization curves for ORR at different Pt/C electrodes (currents normalized to Pt loading in a catalyst layer). Recorded at room temperature in O_2-saturated 1 M H_2SO_4. Rotation speed: 1000 rpm, scan rate: 20 mVs^{-1}.

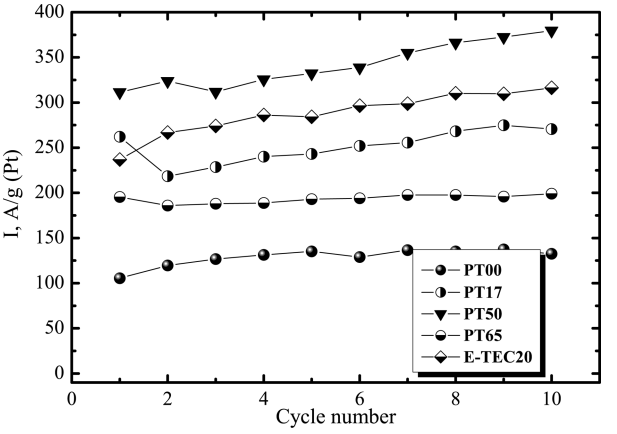

Figure 8. Specific cathode current at E = 0.7 V as a function of cycle number for the prepared Pt/C electrocatalysts (according to results of cyclic voltammetry). 1 M H_2SO_4, O_2 atmosphere.

activity. However, as shown in Figure 6, the mass activity versus D_{111} curve for the prepared Pt/C catalysts (at a potential of 0.7 V) does not follow the expected trend but rather displays a maximum at D_{111} = 2.7 nm. It should be remembered that the reduction in the particle size is accompanied by changes in the particle shape: the fraction of the Pt{100} surfaces decreases, whereas that of the Pt{111} ones increases. According to Markovic et al., the catalytic activity of the Pt single crystals in a medium of H_2SO_4 depends on the surface orientation and increases in the order Pt {111} < Pt {100} < Pt {110}.[28] In such a case, as D_{111} falls down to 3 nm, the total surface area of Pt increases and the catalytic activity enhances, as expected. On further reduction in the particle size, however, a change in the particle shape becomes a predominant factor. The total area of the less active {111} surfaces then increases at the expense of the {100} ones. The result is a drop in the catalytic activity.

In summary, carbon-supported Pt catalysts with an average particle size of 1.8−5.4 nm and metal loading of 20 wt % were prepared by wet synthesis using $NaBH_4$ as a reduction agent. These catalysts were characterized by various techniques revealing a strong anisotropy of the synthesized particle shape. It was found that the average particle size, the GSD dispersion, and the associated unit cell parameter decrease progressively with

dx.doi.org/10.1021/jp1109477 |J. Phys. Chem. C 2011, 115, 5429–5434

increasing concentration of the organic component (DMSO) in the mother solution. Interestingly, the decrease in the particle size also results in a change in the particle shape and an increasing fraction of the less active {111} surface facets. As a consequence, instead of a continuous gain in the catalytic activity with reducing particle size we observe an unexpected loss below a certain critical size where the {111} surfaces become favored. These findings highlight the effect of the particle shape, which seems to prevail over other nanoscale effects and opens new prospects in synthesis toward higher catalytic activities.

AUTHOR INFORMATION

Corresponding Author

*E-mail: i.leontiev@rambler.ru.

ACKNOWLEDGMENT

The authors wish to thank D. Chernyshov and V. Dmitriev for their fruitful discussions (SNBL ESRF) and cooperation during the experimental stage. The work was supported by the Russian Foundation for Basic Research (grants nos. 08-08-00869 and 10-03-00474) and by the Russian Ministry of Education and Science (Contract no. 14.740.11.0371).

REFERENCES

(1) Dekker, M. *Catalysis and Electrocatalysis at Nanoparticle Surfaces*; Wieckowski, A, Savinova, E., Vayenas, C., Eds.; Marcel Dekker: New York; 2003, and references therein.

(2) Sergeev, G. B. *Russ. Chem. Rev.* **2001**, *70*, 809.

(3) Mayrhofer, K. J. J.; et al. *J. Phys. Chem. B* **2005**, *109* (30), 14433.

(4) Hwang, J. T.; Chung, J. S. *Electrochim. Acta* **1993**, *38*, 2715.

(5) Min, M.; et al. *Electrochim. Acta* **2000**, *45*, 4211.

(6) Beard, B. C.; Ross, P. N., Jr *J. Electrochem. Soc.* **1990**, *137*, 336.

(7) (a) Sau, T. K.; Pal, A.; Pal, T. *J. Phys. Chem. B* **2001**, *105* (38), 9266. (b) Schulz, J.; Roucoux, A.; Patin, H. *Chem.—Eur. J.* **2000**, *6* (4), 618. (c) Guterman, V. E.; et al. *Inorg. Mater.* **2009**, *45* (5), 498.

(8) Guterman, V. E.; et al. *Russ. J. Electrochem.* **2007**, *43* (9), 1091.

(9) *Standard Reference Material*, Vol. 674, National Institute of Standards and Technology, Gaithersburg, MD, USA, 1983.

(10) Hammersley, A. P.; Svensson, S. O.; Hanfland, M.; Fitch, A. N.; Hausermann, D. *High Pressure Res.* **1996**, *14*, 235.

(11) Thompson, P.; Cox, D. E.; Hastings, J. B. *J. Appl. Crystallogr.* **1987**, *20*, 79.

(12) Roisnel, T.; Rodriguez-Carvajal J. *WinPLOTR: A Windows Tool for Powder Diffraction Patterns Analysis Materials Science Forum*, Proceedings of the Seventh European Powder Diffraction Conference (EPDIC 7), 2000, *118*, Delhez, R., Mittenmeijer, E.J., Eds.

(13) Leontyev, I. N.; Chernyshov, D.Yu.; Guterman, V. E.; Pachomova, E. V.; Guterman, A. V. *Appl. Catal., A* **2009**, *357*, 1.

(14) Vives, S.; Gaffet, E.; Meunier, C. *Mater. Sci. Eng.* **2004**, *A366*, 229.

(15) Klug, H. P.; Alexander, L. E. *X-ray Diffraction Procedures from Polycrystalline and Amorphous Materials*; John Wiley: New York, 1974.

(16) Williamson, G. K.; Hall, W. H. *Acta Met.* **1953**, *1*, 22.

(17) Pielaszek, R. *J. Alloy. Compd.* **2004**, *382*, 128.

(18) http://www.nanotechnology.sfedu.ru/index.php?page=rus.faculty.projects.

(19) Holland, T. J. B.; Redfern, S. A. T. *J. Appl. Crystallogr.* **1997**, *30*, 84.

(20) Guterman, V. E.; Belenov, S. V.; Dymnikova, O. V.; Lastovina, T. A; Konstantinova, Ya. B.; Prutsakova, N. V. *Inorg. Mater.* **2009**, *45* (5), 498.

(21) (a) Gryaznov, V. G.; et al. *Phys. Rev. B* **1991**, *44*, 42.(b) Gryaznov, V. G.; et al. *Technical Physics Letters* (Pis'ma v Zhurnal Tekhnicheskoi Fiziki) **1989**, *15*, 39.

(22) (a) Peng, Z.; Yang, H. *Nano Today* **2009**, *4*, 143. (b) Tao, A. R.; Habas, S.; Yang, P. *Small* **2008**, *4* (3), 310.

(23) Jiang, Q.; Lu, H. M. *Surf. Sci. Rep.* **2008**, *63*, 427.

(24) (a) Wang, Z. L. *J. Phys. Chem. B* **2000**, *104* (6), 1153. (b) Solla-Gullon, J.; et al. *Phys. Chem. Chem. Phys.* **2008**, *10*, 3689. (c) Narayanan, R.; El-Sayed, M. A. *Nano Lett.* **2004**, *4* (7), 1343.

(25) Vermaak, J. S.; Mays, C. W.; Kuhlmann-Wilsdorf, D. *Surf. Sci.* **1968**, *12*, 128.

(26) Qi, W. H.; et al. *J.Nanoparticle Res.* **2009**, *11*, 575and reference therein..

(27) Frenken, J. W. M.; Stoltze, P. *Phys. Rev. Lett.* **1999**, *82* (17), 3500.

(28) Markovic, N. M.; et al. *Phys. Chem.* **1995**, *99* (11), 3411.